



The role of fused thiophene and naphthalene diimide (NDI) in shaping the optical and electrical properties of donor-acceptor polymers

Klaudia Dang Anh^a, Paloma L. dos Santos^{b,*}, Mana Saeed^c, Mujeeb U. Chaudhry^c,
Ivan H. Bechtold^d, Adam Batycki^a, Anna Drewniak^a, Agata Szlapa-Kula^e,
Przemyslaw Ledwon^{a,**}

^a Department of Physical Chemistry and Technology of Polymers, Faculty of Chemistry, Silesian University of Technology, 44-100, Gliwice, Strzody 9, Poland

^b Department of Electronic and Electrical Engineering, University of Sheffield, Sheffield, S1 3JD, UK

^c Department of Engineering, Durham University, Durham, DH1 3LE, UK

^d Department of Physics, Universidade Federal de Santa Catarina, 88040-900, Florianópolis, SC, Brazil

^e Institute of Chemistry, University of Silesia, 9th Szkolna Street, 40-006, Katowice, Poland

ARTICLE INFO

Keywords:

Donor-acceptor
Conjugated polymers
Fused thiophenes
Naphthalene diimide
Organic semiconductors
OFET

ABSTRACT

Three polymers with general structure (D-A)_n were designed and synthesized to investigate the interaction of strong donors and strong acceptors in polymer chain. They are based on different fused thiophenes (**1Th**: 4,4'-bis(2-ethylhexyl)-cyclopenta [2,1-b:3,4-b']dithiophene; **2Th**: 4,8-bis [(2-ethylhexyl)oxy]benzo [1,2-b:4,5-b'] dithiophene; **3Th**: 4,8-bis(4-fluoro-5-(2-ethylhexyl)-thiophen-2-yl)benzo [1,2-b:4,5-b']bisthiophene) and *N,N'*-bis(2-ethylhexyl)-1,8:4,5-naphthalenetetracarboxydiimide (NDI). Fused benzo- and cyclopenta-thiophene derivatives were selected because they are known for their strong electron-donating properties. NDI was coupled with them in polymer chain because it is one of the best known electron withdrawing units. Such combination of donor and acceptor units is one of the strategies for obtaining low band gap conjugated polymers with semi-conducting properties for many applications. The interaction of donors and acceptors is a key factor determining the properties of such polymers. The electrochemical and spectroscopic measurement were supported by DFT calculations. Moreover, organic field effect transistors (OFET) were fabricated to demonstrate the feasibility of using the newly developed materials in electronic devices.

1. Introduction

We are in an era of growing interest in semiconductors. One of the paths that is currently being chosen for development of semiconductors are n-type organic materials [1,2]. There are much less such materials compared to p-type organic semiconductors. This is because most of these types of materials in the n-doped state spontaneously react with oxygen, leading to rapid degradation of the properties of these types of materials. The next type includes semiconductors of mixed ambipolar nature. Ambipolar semiconductors are promising candidates for organic field effect transistors (OFET) as component of compact organic complementary circuits [3]. In this case, one of the limiting factors is the correct balance of ambipolar hole and electron mobility [4]. In the case

of donor-acceptor (D-A) polymers, we have complex relationships between structure and properties that determine a given type of conductivity [5–7]. Understanding the relationship between the structure of the D-A polymer and its properties is key to the further development of this type of materials.

Naphthalene diimides (NDI) are considered to be one of the most stable electron-withdrawing units [8]. One of the factors that influence its stabilization in ambient conditions is the energy of the LUMO level. Accordingly, the radical anions of some derivatives show good stability in the ambient air atmosphere [9,10]. Such properties in combination with good electrical conductivity of solid films with extended π -stacks make this material potentially interesting for the production of air stable n-type organic semiconductors [11,12]. Among the various NDI

* Corresponding author.

** Corresponding author.

E-mail addresses: klaudiamaidang@gmail.com (K. Dang Anh), p.l.dossantos@sheffield.ac.uk (P.L. dos Santos), mana.saeed@durham.ac.uk (M. Saeed), mujeeb.u.chaudhry@durham.ac.uk (M.U. Chaudhry), ivan.bechtold@ufsc.br (I.H. Bechtold), adambat364@student.polsl.pl (A. Batycki), drewniakaz@gmail.com (A. Drewniak), agata.szlapa-kula@us.edu.pl (A. Szlapa-Kula), przemyslaw.ledwon@polsl.pl (P. Ledwon).

<https://doi.org/10.1016/j.orgel.2024.107058>

Received 24 January 2024; Received in revised form 15 April 2024; Accepted 15 April 2024

Available online 27 April 2024

1566-1199/© 2024 The Authors. Published by Elsevier B.V. This is an open access article under the CC BY license (<http://creativecommons.org/licenses/by/4.0/>).

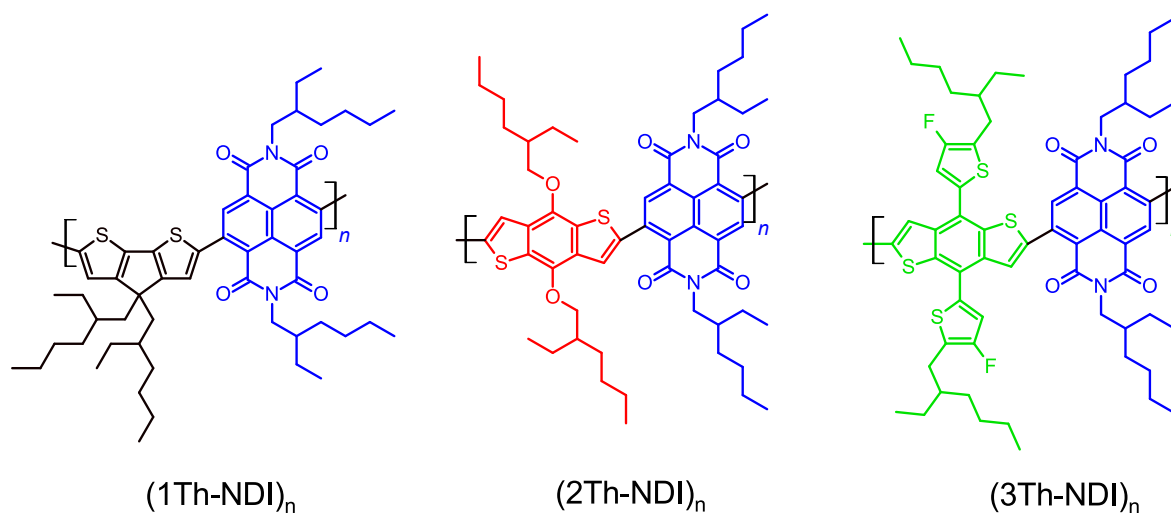


Fig. 1. Structure of (1Th-NDI)_n, (2Th-NDI)_n, (3Th-NDI)_n polymers.

derivatives, we distinguish low molecular weight derivatives and polymers. Both groups of compounds have certain advantages and disadvantages. However, due to their good mechanical properties, polymeric derivatives may be more suitable. In the case of optoelectronic applications such properties as solution deposition, film-forming, flexibility and good semiconductor properties are crucial [13,14]. The analysis of different studies indicates the key role of π -units located between NDI units on the properties of synthesized polymers [15–17]. The analysis of various NDI polymers indicates their wide application possibilities. NDI-based polymers have so far been used in OFETs [18–20] and their various derivatives, e.g. sensors, as acceptors in organic solar cells [21], *n*-type layers in perovskites [21], and many others.

Polythiophenes are particularly often used as building blocks of many conjugated materials. This is related to their electronic properties. In particular, it is worth mentioning the possibilities of controlling the electrical conductivity of many of their derivatives [22]. Commonly, polythiophenes are known to be *p*-type conductive [23]. However, their amphoteric properties are also known. Currently, the main strategy for shaping the electronic properties of conjugated polymers involves the design of the π -conjugated backbone structure by mixing electron-rich and electron-deficient units. Alternating arrangement of electron-donating and electron-accepting units results in strong interaction between these units which in turn leads to a significant change in properties. Wide possibility of modelling these properties is the main advantage of donor-acceptor type of organic semiconductors. Such factors as bond-length, planarity, resonance energy, substituents effects, π -conjugation length, and its structure, intermolecular interactions can be controlled [24]. This may be particularly useful when combined thiophenes with different strong acceptors to obtain new *n*-type polymeric semiconductors [23,25,26]. In the case of planar structures based on thiophenes, this leads to the possibility of using them in *n*-type OFETs [27–29].

Cyclopentadithiophene is known strong electron-donating units which can be used to produce conductive polymers [30]. Thanks to its planar structure, it can effectively increase the coupling length resulting in low bandgap semiconducting materials with high hole mobility [31]. In combination with acceptor units, it may also have an ambipolar character [32]. Benzodithiophene is another example of thiophene fused derivative used to obtain semiconducting polymers [33]. In their case, we see a particularly promising use in organic solar cells [34].

In this work, we present three polymers with three different fused thiophenes acting as electron donors and NDI units acting as electron acceptors (Fig. 1). We show that the use of this type of materials can lead to modification of semiconducting properties. These differences can

affect optical, electrochemical and semiconductor properties in different ways. Moreover, we fabricated and characterized bottom-gated organic field effect transistors (OFET) to demonstrate the feasibility of using the newly developed materials in electronic devices and also to determine their charge transport mobilities. OFETs using (1Th-NDI)_n and (3Th-NDI)_n best performed when tested under $V_{DS} = +40$ V (*N*-type channel) and showed ambipolar character. When tested under $V_{DS} = -40$ V (*P*-type channel) the devices showed *N*-type character.

2. Experimental

2.1. Synthesis

The polymers with different fused thiophene 1Th, 2Th, 3Th and naphthalene diimide NDI were synthesized using typical Stille coupling reactions. All reagents were purchased from Sigma-Aldrich, TCI, Acros Organics and Ossila. The reaction scheme and synthesis details are provided in supporting information.

2.2. Characterization

Molecular weight and dispersities (\bar{D}) were determined by GPC measurement using Agilent 1260 Infinity series equipped with a differential refractometer MDS RI Detector. Measurements were carried out in HPLC grade CH_2Cl_2 as a solvent with a flow rate of 0.8 ml/min at 45 °C, calibrated using linear polystyrene standards (580–1 390 000 g/mol). Thermogravimetric analysis (TGA) was carried out using TGA 8000 thermogravimetric analyzer.

Cyclic voltammetry was performed on Autolab PGSTAT 100 N potentiostat in three electrode cell, with platinum wire as working electrode and platinum spiral as counter electrode. A silver wire was used as a pseudo-reference electrode. Potential was measured against ferrocene used as internal standard. Cyclic voltammetry experiments of 1 mg/ml solutions of each polymer were carried out in 0.1 M Bu_4NPF_6 (TCI) in DCM (Purechem) as supporting electrolyte, at a potential scan rate of 0.1 V/s. Cyclic voltammetry of polymer films was carried out in 0.1 M Bu_4NPF_6 (TCI) in ACN (99.8 % Sigma Aldrich, HPLC grade) supporting electrolyte, at a potential scan rate of 0.1 V/s 1 mg mL⁻¹ polymers solution were drop coated on Pt disc electrode at 40 °C. Electrolyte solutions were degassed with argon prior to measurement.

UV-Vis spectra measurements were performed using PerkinElmer UV-Vis-NIR Lambda 1050 spectrometer. Absorption of polymers was measured in solution and in films. 0.01 mg mL⁻¹ solution of polymers in DCM (Pure chem) were used. 1 mg mL⁻¹ DCM solution of polymers were

Table 1
Basic properties of polymers.

Polymer	M_n [kDa]	\bar{D}	$T_{d5\%}$ °C
(1Th-NDI) _n	22.67	2.36	444
(2Th-NDI) _n batch 1*	22.74	3.23	376
(2Th-NDI) _n batch 2a	26.51	3.33	
(2Th-NDI) _n batch 2b	31.77	2.48	
(2Th-NDI) _n batch 3	32.96	2.21	
(3Th-NDI) _n	55.07	2.81	374

M_n - number average molecular weight; \bar{D} - dispersity index; $T_{d5\%}$ - the thermal decomposition temperature; * different purification procedures and batch of monomer: batch 1 and batch 2a without Soxlet extraction using DCM; batch 2b and batch 3 with Soxlet extraction using DCM.

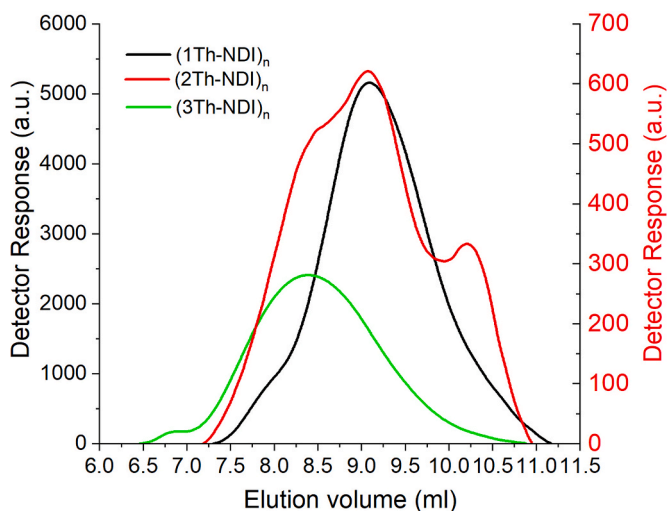


Fig. 2. GPC curves for (1Th-NDI)_n, (2Th-NDI)_n from batch 1, (3Th-NDI)_n. Full GPC curves are provided in SI.

spin coated on glass surface.

The X-Ray diffraction experiments were realized with the X'Pert-PRO (PANalytical) diffractometer system using the linear monochromatic CuK α 1 beam ($\lambda = 1.5405 \text{ \AA}$), with an applied power of 1.2kVA. The scans were performed in continuous mode from 2° to 30° (2 θ angle) and the diffracted radiation collected with the X'Celerator detector. Drop-casting films were prepared with (1Th-NDI)_n, (2Th-NDI)_n and (3Th-NDI)_n.

2.3. Devices

OFETs were fabricated using the following structure: Si⁺⁺/SiO₂ (300 nm) substrates (purchased from Active Business Company GmbH) were pre cleaned in IPA and Acetone (ultrasonic bath 15 min each); PMMA (SigmaAldrich; $M_w \sim 120 \text{ k}$) layer were spin-coated from toluene solution (10 mg/ml in toluene) using the parameters: 2000 rpm; 15000 rpm/s; 30s and annealed for 20 min annealing at 100°C to remove the solvent. Then, polymers were spin-coated from Chlorobenzene solutions ($\sim 10 \text{ mg/ml}$) using the parameters: 2000 rpm; 15000 rpm/s; 30s and annealed for 20 min at 100°C . Finally, Gold (50 nm) was thermally evaporated (chamber at 10–6 mbar). Device channel dimension was: width 3 mm x length 50 μm . The electrical performance of the devices was characterized using a Keysight B1500A Semiconductor device analyzer and probe station. All devices were tested inside a nitrogen glovebox.

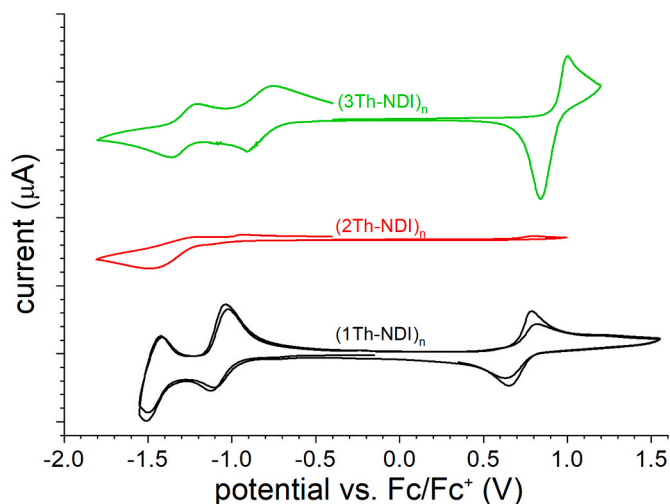


Fig. 3. Cyclic Voltammetry of polymers deposited on Pt plate recorded in 0.1 M Bu₄NPF₆/ACN electrolyte.

3. Results and discussion

3.1. Synthesis and characterization

All polymers were synthesized using a typical Stille coupling. GPC results and the thermal properties of polymers are summarised in Table 1. GPC measurement reveals that polymers with number-average molar mass M_n ranging from 22.67 kDa to 55.07 kDa were obtained.

A multimodal molecular weight distribution is evident for (2Th-NDI)_n as illustrated in Fig. 2. This distribution can significantly impact the performance of conjugated polymer films, especially the fraction with lower molecular weight. The synthesis of this polymer was repeated twice more using new batches of monomers. Batch 2 was further subdivided into two parts 2a and 2b to assess the influence of purification via Soxlet extraction on the multimodal molecular weight distribution and dispersibility (\bar{D}). DCM was used because it is often used to elute oligomers. In batch 2a, Soxhlet extraction involved methanol, acetone, and hexane, while in batch 2b, DCM extraction was additionally employed. The DCM extraction of oligomers was terminated after 24 h when no further coloration of the solvent was observed. Comparison of the GPC profiles of batches 2a and 2b reveals that DCM employment led to higher M_n and lower \bar{D} . However, as depicted in Fig. S5-2a and Fig. S5-2b, the fraction with the lowest mass fraction (M_n approx. 7 kDa) remains present in the polymer. Batch 3 replicated the entire procedure of batch 2b, resulting in a polymer with only minor deviations in M_n and \bar{D} , along with a similar content of lower mass fractions compared to batch 2b. This behaviour can be attributed to the robust π - π interaction between adjacent chains, hindering the complete removal of polymer chains with lower mass. Confirmation of π - π interaction in the solid-state is supported by UV-vis spectra, as described in the Optical Properties section. Additionally, XRD measurements on polymer films confirmed the ordering of (2Th-NDI)_n, as discussed in the X-ray Diffraction section.

As indicated by the values of the thermal decomposition temperatures ($T_{d5\%}$), all polymers exhibit excellent thermal stability, ranging from 374 to 444°C . DSC measurements do not reveal any pronounced thermal transitions. This characteristic is common in polymers with an extensive donor-acceptor structure.

3.2. Electrochemical properties

Electronic structure, electronic band gap (E_g), highest occupied molecular orbital (HOMO), lowest unoccupied molecular orbital (LUMO), electric conductivity are among the most important properties

Table 2
Electrochemical and optical properties of polymers.

Polymer	E _{onset red} film [V]	E _{onset ox} film [V]	EA [eV]	IP [eV]	λ _{CHCl₃} [nm]	λ _{solid} [nm]	ΔE _{gel} [eV]	ΔE _{gop} CHCl ₃ [eV]	ΔE _{gop} solid [eV]
(1Th-NDI) _n	-0.93	0.65	4.35	5.75	850	917	1.58	1.46	1.35
(2Th-NDI) _n	-0.95	0.68	4.15	5.78	767	804	1.63	1.62	1.54
(3Th-NDI) _n	-0.73	0.91	4.13	6.01	703	775	1.64	1.76	1.60

E_{onset red} - reduction onset potential, E_{onset ox} - oxidation onset potential, IP = |e⁻|(5.1+E_{ox onset}), ^bEA = |e⁻|(5.1+E_{red onset}), ^bΔE_{gel} = IP-EA.

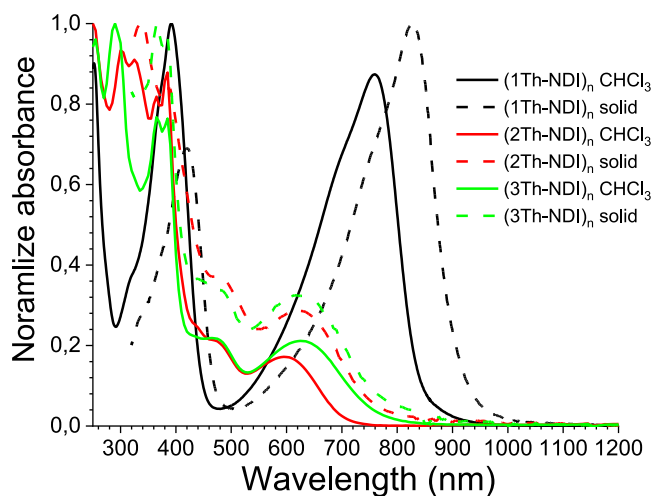


Fig. 4. UV-Vis-NIR spectra of polymers in CHCl₃ solution 0.01 mg/ml and solid films.

of organic semiconductors [35]. Electrochemical properties were determined using cyclic voltammetry measurements of polymer solutions and layers. CV of spin-coated polymer films are shown in Fig. 3. Electrochemical properties are summarised in Table 2. Significant differences in the properties of the tested polymers can be observed in the CV during oxidation. CV shows a clear first oxidation redox pair peak for polymers (1Th-NDI)_n and (3Th-NDI)_n. For polymer (2Th-NDI)_n, there is only a slight increase in current, which may indicate the oxidation of the polymer layer located directly on the surface of the platinum electrode. These differences clearly indicate that in the cases of (1Th-NDI)_n and (3Th-NDI)_n, the transport of positive charges and then oxidation of polymers away from the electrode occurs more easily than in the case of polymer (2Th-NDI)_n.

The beginning of the oxidation and reduction potential is related to the electronic properties of the tested polymers. The onset oxidation potential (E_{onset ox}) is closely related to the energy of the HOMO orbital, while the onset reduction potential (E_{onset red}) is related to the energy of the LUMO orbital. Significant differences in oxidation onset potentials are observed. The oxidation of (1Th-NDI)_n and (2Th-NDI)_n starts at 0.65 and 0.68 V, respectively, while for (3Th-NDI)_n, it begins at 0.91 V. Similar dependencies are observed for reduction potentials. The reduction onset potential for (1Th-NDI)_n and (2Th-NDI)_n is -0.93 and -0.95 V, respectively, while for (3Th-NDI)_n, it is -0.73 V. This effect can be attributed to the electron-withdrawing nature of fluorine substituents in (3Th-NDI)_n. Electrochemical energy gap (ΔE_{gel}) show clear differences depending on the fused thiophene used. (1Th-NDI)_n has a smaller ΔE_{gel} than the other two. This is mainly due to the lower ionization potential, which is related to the increased energy of the HOMO orbital. This is also confirmed by DFT calculations which are presented in the following sections.

Table 3
HOMO and LUMO energies and band gaps (E_g).

compound	HOMO [eV]	LUMO [eV]	E _g [eV]
(1Th-NDI) ₁	-5.62	-3.63	1.98
(1Th-NDI) ₂	-5.49	-3.71	1.78
(1Th-NDI) ₃	-5.44	-3.74	1.70
(2Th-NDI) ₁	-5.77	-3.71	2.06
(2Th-NDI) ₂	-5.78	-3.76	2.02
(3Th-NDI) ₁	-5.84	-3.71	2.13
(3Th-NDI) ₂	-5.84	-3.76	2.08

3.3. Optical properties

Fig. 4 presents the UV-VIS absorption spectra of the synthesized polymers in both CHCl₃ solution and the solid state. In all instances, a bathochromic shift is evident when comparing the solid layers to the solutions. This phenomenon is likely attributed to aggregation and strong interactions between polymer chains. π-Stacking, a phenomenon with a profound impact, influences various properties of NDI-based molecules, including electrical conductivity, redox stability, photoluminescence, and absorption range [36–39].

All spectra exhibit a complex structure. The spectra in the ultraviolet range display typical transitions characteristic of fused molecules, such as NDI. In the case of (1Th-NDI)_n, a strong absorption peak is observed in the visible and near-infrared parts of the spectrum, while the absorption in the visible range is weaker for (2Th-NDI)_n and (3Th-NDI)_n. These properties are explained by DFT calculations. Calculations clearly indicate that the reason is the difference overlapping between the HOMO and LUMO orbitals. In the case of compounds (2Th-NDI)_n and (3Th-NDI)_n, there is a strong separation of these orbitals, while for (1Th-NDI)_n there is partial overlap of the HOMO and LUMO orbitals.

3.4. DFT calculations

To better understand the effect of different thiophene units, DFT calculations were performed. The calculations used the exchange hybrid correlation of the B3LYP functional and the 6-311 + G** basis for all atoms. The calculations were carried out using the Gaussian 16 program [40]. Simulated geometries of obtained compounds were optimized in a vacuum. To simplify calculations, methyl units were used in the compound structures instead of aliphatic chains. Based on the optimized geometries, molecular frontier orbitals were calculated in acetonitrile for both the monomer and the oligomers. The values of HOMOs, and LUMOs, and band gaps (E_g) are summarised in Table 3.

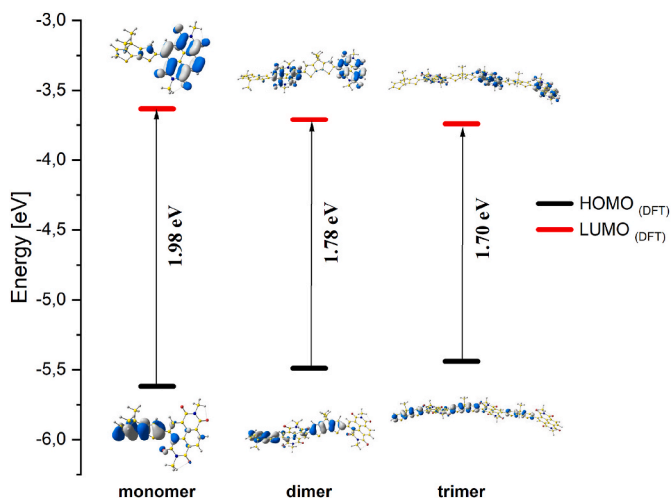
Contour plots of HOMO and LUMO for dimers are collected in Table 4. In the case of monomers (2Th-NDI)₂ and (3Th-NDI)₂, a clear division between the HOMO and LUMO positions is visible. In each case, the HOMO orbital includes substituents with thiophene fragments, while the LUMO is located on NDI. Similarly for monomers (2Th-NDI)₂ and (3Th-NDI)₂, these orbitals are localised on a selected molecule fragment: HOMO on fused thiophene moieties and LUMO on NDI moieties (Table S1).

The resulting HOMO and LUMO orbitals for the monomer (1Th-NDI)₁, dimer (1Th-NDI)₂, and trimer (1Th-NDI)₃ are depicted in Fig. 5.

Table 4

Graphical representations of HOMO and LUMO contours, calculated at B3LYP/6-311 + G** level of theory.

compound	HOMO	LUMO
(1Th-NDI) ₂		
(2Th-NDI) ₂		
(3Th-NDI) ₂		

Fig. 5. Energy-level diagram representing the selected highest occupied and lowest unoccupied molecular orbitals for compounds (1Th-NDI)₁, (1Th-NDI)₂, (1Th-NDI)₃.

In the case of this (1Th-NDI)_n series of compounds the HOMO orbital is delocalized not only on 1Th units but also on NDI units, which may facilitate energy transfer. This effect clearly affects the HOMO energy and E_g values. Simultaneously, overlapping of HOMO and LUMO affects the absorption of light in the Vis and NIR range (Fig. 4). The intense absorption in the VIS-NIR range observed for (1Th-NDI)_n is attributed to a greater overlap between the HOMO and LUMO orbitals compared to polymers (2Th-NDI)_n and (3Th-NDI)_n.

The energy gap values are in the order (1Th-NDI)₂ (1.78 eV) < (2Th-NDI)₂ (2.02 eV) < (3Th-NDI)₂ (2.08 eV). The calculation results are consistent with the experimental results obtained for UV measurements and cyclic voltammetry. Electrochemical and optical energy gaps (ΔE_{g,el} and ΔE_{g,opt}) using different methods show the same trend.

The angles between NDI and Th were also analysed for all monomers (Table S2). These compounds do not show significant differences in

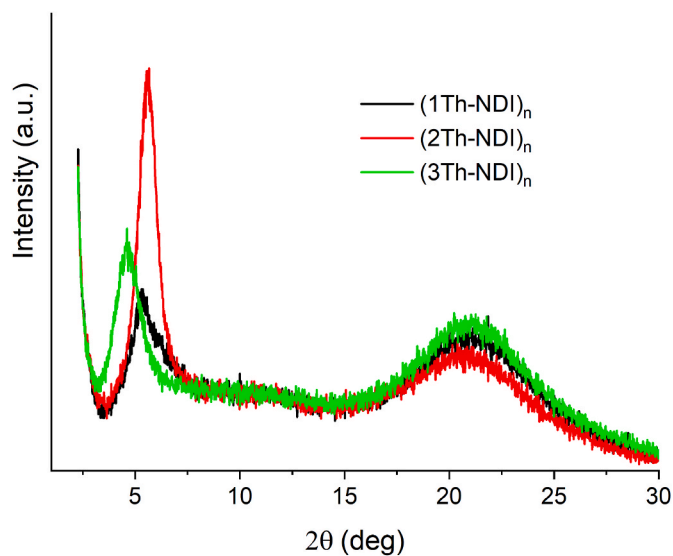


Fig. 6. XRD spectra of polymer films.

these parameters. However, the tendency of the angle deviation is (1Th-NDI)₂ (115.48°) < (3Th-NDI)₂ (115.76°) < (2Th-NDI)₂ (115.82°).

3.5. X-ray diffraction

XRD experiments were carried out to investigate the polymer structure of (1Th-NDI)_n, (2Th-NDI)_n and (3Th-NDI)_n. The films exhibited a diffraction peak at low angle region, corresponding to the lamellar packing distance, with a broad halo around 22° (approx. 4.2 Å) related to the liquid-like order of the lateral aliphatic chains (Fig. 6). The lamellar packing distance is larger for (3Th-NDI)_n, 19.1 Å, which is consistent with the additional lateral groups of this molecule. The full width at half maximum (FWHM) indicates the order of crystallinity of the polymeric films. As smaller FWHM, more intense is the peak, and consequently, more organized are the molecules in the film. The values

Table 5
Structure properties of polymer films obtained with XRD.

Compound	d (Å)	Halo (Å)	FWHM (Å)
(1Th-NDI) _n	16.6	4.2	4.3
(2Th-NDI) _n	15.7	4.2	2.8
(3Th-NDI) _n	19.1	4.1	4.8

show that (2Th-NDI)_n is the most organized. Table 5 displays the obtained parameters.

3.6. OFETs

To investigate the electrical properties of the different materials, bottom-gated OFET devices were fabricated and characterized under an inert atmosphere (Fig. 7a). Device structures were as follows: Si⁺⁺/SiO₂ (300 nm) substrates/polymethyl methacrylate (PMMA)/Polymer/Gold (50 nm), where Si⁺⁺ acts as substrate and gate electrode, SiO₂ as dielectric, PMMA as smooth layer to ensure the quality of the semiconductor/dielectric interface, polymers as semiconductor layer and gold electrodes as source and drain.

Transfer characteristics were obtained in the saturation region by keeping V_{DS} constant at +40 V (gate-to-source voltage (V_{GS}) sweeping between -20 V and +40 V – Fig. 7b) as well as at V_{DS} constant of -40 V (V_{GS} sweeping between -40 V and 20 V – Fig. 7c) to acquire device performance under *N*-type channel and *P*-type channel, respectively. In both cases, 0.5 V V_{GS} interval were used.

The electrical parameters of the OFET, namely saturation hole mobility (μ_{sat}) and threshold voltage (V_{TH}) are shown in Table 6 for (3Th-NDI)_n and (1Th-NDI)_n (see SI11 for fitting). Devices produced with (2Th-NDI)_n worked at very low currents and were not satisfactory devices (See SI12). We used the standard Equation (1) to calculate μ_{sat} .

$$\mu_{sat} = \frac{2L}{WCi} \left(\frac{\partial \sqrt{I_{DS}}}{\partial V_{GS}} \right)^2 \quad (1)$$

where μ_{sat} is the charge carrier mobility, L and W are the length and width of the accumulation channel, Ci is the gate capacitance per unit area of the dielectric layer. μ is obtained by taking the partial derivative of $\sqrt{I_{DS}}$ with respect to V_{GS}. V_{th} can be extracted through extrapolation of the linear region of the square root of drain current $\sqrt{I_{DS}}$.

(1Th-NDI)_n and (3Th-NDI)_n OFETs best performed when tested under V_{DS} = +40 V (*N*-type channel) with low threshold voltage ((3Th-NDI)_n = -1.3 V; (1Th-NDI)_n = 0.44 V) and ambipolar character. The carrier mobilities under this testing condition were calculated to be (3Th-NDI)_n = 1.18 × 10⁻⁵ cm²/Vs; (1Th-NDI)_n = 6.81 × 10⁻⁶ cm²/Vs. Ambipolar behaviour are attractive in the field of low-cost and

flexible electronics, as it allows devices fabrication utilizing only one semiconductor materials and one electrode material, simplifying device layout designs, however, the mobilities are low compared to state-of-the-art devices. Regarding the threshold voltages, i.e. the minimum V_{GS} that is needed to create a conducting path between the source and drain terminals, its desirable to be as close to zero as possible. A lower threshold voltage can lead to improved device performance, by providing faster switching speeds and higher on/off current ratios. This is desirable for applications where high-speed switching operation is necessary as well as precise control of current flow.

(1Th-NDI)_n and (3Th-NDI)_n OFETs were also tested under V_{DS} = -40 V (*P*-type channel), however using these testing conditions, the devices showed *N*-type character rather than ambipolar as well as very large values of threshold voltages. We speculate that the threshold voltages are likely to be even higher if the testing range exceed -40 V and better estimation could be obtained.

Output curves were obtained for both devices under the *N*-type channel and *P*-type channel (see SI4) show a decent saturation behaviour.

4. Conclusions

Three polymers based on NDI acting as electron-acceptor unit and different fused thiophenes 1Th, 2Th and 3Th acting as electron units were synthesized and characterized. Despite slight differences in the fused thiophene structure, the polymers exhibited different physico-chemical properties. The complex relationships between the structure of polymers and their properties seem particularly important for polymer layers. For all 3 polymers, ordering was observed in the solid layer demonstrated by significant shifts in the UV-VIS-NIR spectra in the solution and the solid state. This indicate strong interactions between adjacent chains in the solid layer. Especially (1Th-NDI)_n showed a significant shift of absorption maximum from 756 nm in chloroform to 828 nm in solid state. The ordering was confirmed by XRD measurement. Also the energy gap determined electrochemically, optically, and by theoretical calculations shows differences depending on the used thiophene derivative. These differences were explained using theoretical calculations. DFT calculations indicate different degrees of overlap

Table 6
Merits of (1Th-NDI)_n and (3Th-NDI)_n OFET devices. Fitted curves are shown in SI1.

OFET	V _{DS} = +40 V		V _{DS} = -40 V	
	μ_{sat} (cm ² /Vs)	V _{th} (V)	μ_{sat} (cm ² /Vs)	V _{th} (V)
(1Th-NDI) _n	6.81 × 10 ⁻⁶	0.44	3.29 × 10 ⁻⁵	-40
(3Th-NDI) _n	1.18 × 10 ⁻⁵	-1.3	1.28 × 10 ⁻⁵	-48.6

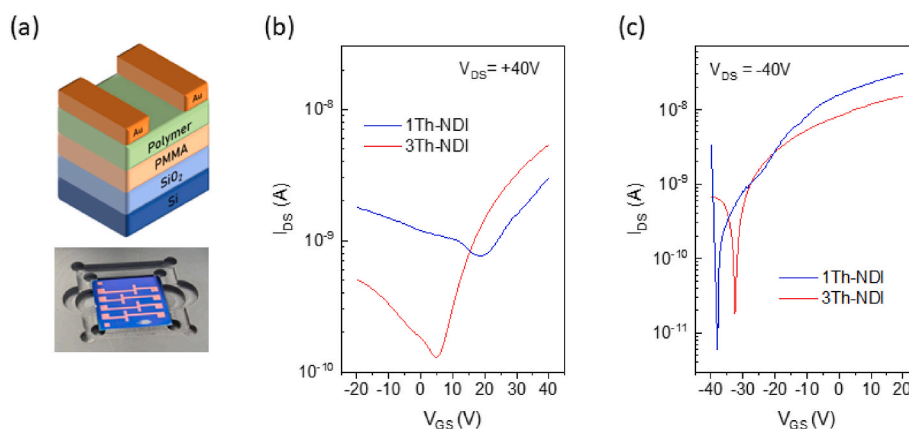


Fig. 7. (a) OFET device structure and photo. Transfer curves obtained from devices using (1Th-NDI)_n and (3Th-NDI)_n as semiconductor layers using V_{DS} of (b) +40 V and (c) -40 V.

between HOMO and LUMO orbitals for different polymer structures. In the case of (1Th-NDI)_n, delocalization of the HOMO orbital into fused thiophene and NDI units is observed. Different types of Organic field effect transistors (OFET) based on studied polymers were fabricated. The results show the typical *N*-type nature of semiconductors based on (1Th-NDI)_n and (3Th-NDI)_n when tested under $V_{DS} = -40$ V (*P*-type channel). In the case of (2Th-NDI)_n, a deterioration of semiconductor properties was observed, which can be interpreted as a significant influence of the multimodal mass distribution.

CRedit authorship contribution statement

Klaudia Dang Anh: Writing – original draft, Investigation. **Paloma L. dos Santos:** Writing – review & editing, Writing – original draft, Investigation. **Mana Saeed:** Writing – original draft, Investigation. **Mujeeb U. Chaudhry:** Supervision. **Ivan H. Bechtold:** Writing – original draft, Investigation. **Adam Batycki:** Investigation. **Anna Drewniak:** Writing – original draft, Investigation. **Agata Szlapa-Kula:** Writing – original draft, Investigation. **Przemyslaw Ledwon:** Writing – review & editing, Writing – original draft, Methodology, Investigation, Formal analysis, Data curation, Conceptualization.

Declaration of generative AI and AI-assisted technologies in the writing process

During the preparation of this work the author PL used ChatGPT in order to improve language. After using this tool/service, the author(s) reviewed and edited the content as needed and take(s) full responsibility for the content of the publication.

Declaration of competing interest

The authors declare that they have no known competing financial interests or personal relationships that could have appeared to influence the work reported in this paper.

Data availability

Data will be made available on request.

Acknowledgements

Authors acknowledge the EU's Horizon 2020 for funding the OCTA project under grant agreement No 778158, INCT/INEO, CNPq, CAPES and FAPESC. Research work supported from the funds for science in 2018–2023 allocated to the implementation of an international co-financed project by the Polish Ministry of Education and Science. PLDS acknowledges Royal Society support award RG\R1\241188. The XRD experiments were carried out in the Laboratório de Difração de Raios X (LDRX/UFSC). We thank dr Sylwia Waskiewicz for GPC measurement.

Appendix A. Supplementary data

Supplementary data to this article can be found online at <https://doi.org/10.1016/j.orgel.2024.107058>.

References

- S. Griggs, A. Marks, H. Bristow, I. McCulloch, *n*-Type organic semiconducting polymers: stability limitations, design considerations and applications, *J. Mater. Chem. C* 9 (2021) 8099–8128, <https://doi.org/10.1039/D1TC02048J>.
- Y. Chen, X. Liang, H. Yang, Q. Wang, X. Zhou, D. Guo, S. Li, C. Zhou, L. Dong, Z. Liu, Z. Cai, W. Chen, L. Tan, Strong near-infrared solid emission and enhanced *N*-type mobility for poly(naphthalene diimide) vinylene by a random polymerization strategy, *Macromolecules* 52 (2019) 8332–8338, <https://doi.org/10.1021/acs.macromol.9b01848>.
- C. Lin, B. Peng, J. Wu, Z. Huang, M. Chen, D. Hu, S. Ke, B.C.K. Tee, H. Li, Ambipolar organic field-effect transistors and complementary circuits based on single crystals with alcohol treatment, *Adv. Electron. Mater.* 8 (2022), <https://doi.org/10.1002/aelm.202200557>.
- S. Cheng, S.H. Yu, S.-K. Kwon, D.S. Chung, Y.-H. Kim, High-performance ambipolar benzodifurandione-based donor-acceptor copolymer with balanced hole and electron mobility, *Dyes Pigments* 162 (2019) 481–486, <https://doi.org/10.1016/j.dyepig.2018.10.038>.
- Z. Chen, W. Li, M.A. Sabuj, Y. Li, W. Zhu, M. Zeng, C.S. Sarap, M.M. Huda, X. Qiao, X. Peng, D. Ma, Y. Ma, N. Rai, F. Huang, Evolution of the electronic structure in open-shell donor-acceptor organic semiconductors, *Nat. Commun.* 12 (2021) 5889, <https://doi.org/10.1038/s41467-021-26173-3>.
- Y. Lei, P. Deng, J. Li, M. Lin, F. Zhu, T.-W. Ng, C.-S. Lee, B.S. Ong, Solution-processed donor-acceptor polymer nanowire network semiconductors for high-performance field-effect transistors, *Sci. Rep.* 6 (2016) 24476, <https://doi.org/10.1038/srep24476>.
- X. Zhu, S. Zhang, Y. Zhou, S. Han, Ambipolar polymers for transistor applications, *Polym. Int.* 70 (2021) 358–366, <https://doi.org/10.1002/pi.6006>.
- J. Shukla, P. Mukhopadhyay, Synthesis of functionalized naphthalene diimides and their redox properties, *Eur. J. Org. Chem.* 2019 (2019) 7770–7786, <https://doi.org/10.1002/ejoc.201901390>.
- S.B. Schmidt, M. Hönig, Y. Shin, M. Cassinelli, A. Perinot, M. Caironi, X. Jiao, C. R. McNeill, D. Fazzi, T. Biskup, M. Sommer, Radical anion Yield, stability, and electrical conductivity of naphthalene diimide copolymers *n*-doped with tertiary amines, *ACS Appl. Polym. Mater.* 2 (2020) 1954–1963, <https://doi.org/10.1021/acscpm.0c00151>.
- C. Wiberg, L. Evenäs, M. Busch, E. Ahlberg, Naphthalene diimides (NDI) in highly stable pH-neutral aqueous organic redox flow batteries, *J. Electroanal. Chem.* 896 (2021) 115224, <https://doi.org/10.1016/j.jelechem.2021.115224>.
- Y.H. Ha, J.G. Oh, S. Park, S.-K. Kwon, T.K. An, J. Jang, Y.-H. Kim, Novel naphthalene-diimide-based small molecule with a bithiophene linker for use in organic field-effect transistors, *Org. Electron.* 63 (2018) 250–256, <https://doi.org/10.1016/j.orgel.2018.09.037>.
- T. He, M. Stolte, F. Würthner, Air-stable *n*-channel organic single crystal field-effect transistors based on microribbons of core-chlorinated naphthalene diimide, *Adv. Mater.* 25 (2013) 6951–6955, <https://doi.org/10.1002/adma.201303392>.
- M. Al Kobaisi, S.V. Bhosale, K. Latham, A.M. Raynor, S.V. Bhosale, Functional naphthalene diimides: synthesis, properties, and applications, *Chem. Rev.* 116 (2016) 11685–11796, <https://doi.org/10.1021/acs.chemrev.6b00160>.
- S.V. Bhosale, M. Al Kobaisi, R.W. Jadhav, P.P. Morajkar, L.A. Jones, S. George, Naphthalene diimides: perspectives and promise, *Chem. Soc. Rev.* 50 (2021) 9845–9998, <https://doi.org/10.1039/D0CS00239A>.
- S. Lee, G.S. Lee, M. Kang, Y.H. Ha, Y. Kim, D.S. Chung, High-performance and high-stability all-polymer photomultiplication-type organic photodiode using an NDI-based polymer acceptor with precisely controlled backbone planarity, *Adv. Funct. Mater.* 32 (2022), <https://doi.org/10.1002/adfm.202204383>.
- K. Kranthiraja, A. Saeki, Impact of sequential fluorination of donor and/or acceptor polymers on the efficiency and morphology of all-polymer solar cells, *ACS Appl. Polym. Mater.* 3 (2021) 2759–2767, <https://doi.org/10.1021/acscpm.1c00288>.
- D. Zhao, D. Kim, S. Ghosh, G. Wang, W. Huang, Z. Zhu, T.J. Marks, I. Zozoulenko, A. Facchetti, Mechanical, morphological, and charge transport properties of NDI polymers with variable built-in π -conjugation lengths probed by simulation and experiment, *Adv. Funct. Mater.* (2023), <https://doi.org/10.1002/adfm.202310071>.
- A. Nyga, T. Kaihara, T. Hosono, M. Sipala, P. Stachelek, N. Tohnai, S. Minakata, L. E. de Sousa, P. de Silva, P. Data, Y. Takeda, Dual-photofunctional organogermanium compound based on donor-acceptor-donor architecture, *Chem. Commun.* 58 (2022) 5889–5892, <https://doi.org/10.1039/D2CC01568D>.
- A. Nyga, S. Izumi, H.F. Higginbotham, P. Stachelek, S. Pluczyk, P. de Silva, S. Minakata, Y. Takeda, P. Data, Electrochemical and spectroelectrochemical comparative study of macrocyclic thermally activated delayed fluorescent compounds: molecular charge stability vs OLED EQE roll-off, *Asian J. Org. Chem.* 9 (2020) 2153–2161, <https://doi.org/10.1002/ajoc.202000475>.
- S. Nam, S.G. Hahm, D. Kim, H. Kim, T. Sajoto, M. Ree, S.R. Marder, T. D. Anthopoulos, D.D.C. Bradley, Y. Kim, Pronounced side chain effects in triple bond-conjugated polymers containing naphthalene diimides for *n*-channel organic field-effect transistors, *ACS Appl. Mater. Interfaces* 10 (2018) 12921–12929, <https://doi.org/10.1021/acscami.8b01196>.
- Z. Genene, W. Mammo, E. Wang, M.R. Andersson, Recent advances in *n*-type polymers for all-polymer solar cells, *Adv. Mater.* 31 (2019), <https://doi.org/10.1002/adma.201807275>.
- Y. Liu, Y. Liu, X. Zhan, High-mobility conjugated polymers based on fused-thiophene building blocks, *Macromol. Chem. Phys.* 212 (2011) 428–443, <https://doi.org/10.1002/macp.201000677>.
- Y. Sun, X. Lu, S. Lin, J. Kettle, S.G. Yeates, A. Song, Polythiophene-based field-effect transistors with enhanced air stability, *Org. Electron.* 11 (2010) 351–355, <https://doi.org/10.1016/j.orgel.2009.10.019>.
- M.C. Scharber, N.S. Sariciftci, Low band gap conjugated semiconducting polymers, *Adv. Mater. Technol.* 6 (2021) 2000857, <https://doi.org/10.1002/admt.202000857>.
- H. Sun, X. Guo, A. Facchetti, High-performance *n*-type polymer semiconductors: applications, recent development, and challenges, *Chem* 6 (2020) 1310–1326, <https://doi.org/10.1016/j.chempr.2020.05.012>.
- X. Ding, D.K. Tran, D. Kuzuhara, T. Koganezawa, S.A. Jenekhe, Comparative study of selenophene- and thiophene-containing *n*-type semiconducting polymers for

- high performance all-polymer solar cells, *ACS Appl. Polym. Mater.* 3 (2021) 49–59, <https://doi.org/10.1021/acsapm.0c00772>.
- [27] A. Velusamy, S.N. Afraj, S. Yau, C. Liu, Y. Ezhumalai, P. Kumaresan, M. Chen, Fused thiophene based materials for organic thin-film transistors, *J. Chin. Chem. Soc. (Taipei, Taiwan)* 69 (2022) 1253–1275, <https://doi.org/10.1002/jccs.202200214>.
- [28] X.-C. Li, H. Sirringhaus, F. Garnier, A.B. Holmes, S.C. Moratti, N. Feeder, W. Clegg, S.J. Teat, R.H. Friend, A highly π -stacked organic semiconductor for thin film transistors based on fused thiophenes, *J. Am. Chem. Soc.* 120 (1998) 2206–2207, <https://doi.org/10.1021/ja9735968>.
- [29] Z. Xue, S. Chen, N. Gao, Y. Xue, B. Lu, O.A. Watson, L. Zang, J. Xu, Structural design and applications of stereoregular fused thiophenes and their oligomers and polymers, *Polym. Rev.* 60 (2020) 318–358, <https://doi.org/10.1080/15583724.2019.1673404>.
- [30] M. Planells, B.C. Schroeder, I. McCulloch, Effect of chalcogen atom substitution on the optoelectronic properties in cyclopentadithiophene polymers, *Macromolecules* 47 (2014) 5889–5894, <https://doi.org/10.1021/ma5014308>.
- [31] M. Li, C. An, W. Pisula, K. Müllen, Cyclopentadithiophene–benzothiadiazole donor–acceptor polymers as prototypical semiconductors for high-performance field-effect transistors, *Acc. Chem. Res.* 51 (2018) 1196–1205, <https://doi.org/10.1021/acs.accounts.8b00025>.
- [32] W. Pisula, H. Tsao, D. Dudenko, D. Cho, S. Puniredd, Y. Zhao, A. Mavrinskiy, J. Shu, M. Hansen, M. Baumgarten, K. Müllen, Solid-state organization and ambipolar field-effect transistors of benzothiadiazole-cyclopentadithiophene copolymer with long branched alkyl side chains, *Polymers* 5 (2013) 833–846, <https://doi.org/10.3390/polym5020833>.
- [33] H. Yao, L. Ye, H. Zhang, S. Li, S. Zhang, J. Hou, Molecular design of benzodithiophene-based organic photovoltaic materials, *Chem. Rev.* 116 (2016) 7397–7457, <https://doi.org/10.1021/acs.chemrev.6b00176>.
- [34] F.A. Angel, M.B. Camarada, I.A. Jessop, Computational chemistry advances on benzodithiophene-based organic photovoltaic materials, *Crit. Rev. Solid State Mater. Sci.* 48 (2023) 333–360, <https://doi.org/10.1080/10408436.2022.2052798>.
- [35] U.W. Pohl, *Electronic Properties of Organic Semiconductors*, 2020, pp. 177–205, https://doi.org/10.1007/978-3-030-43869-2_5.
- [36] A. Drewniak, M. Tomczyk, L. Hanusek, A. Mielanczyk, K. Walczak, P. Nitschke, B. Hajduk, P. Ledwon, The effect of aromatic diimide side groups on the π -conjugated polymer properties, *Polymers* 10 (2018) 487, <https://doi.org/10.3390/polym10050487>.
- [37] V. Singh, S. Kwon, Y. Choi, S. Ahn, G. Kang, Y. Yi, M.H. Lim, J. Seo, M. Baik, H. R. Byon, Controlling π – π interactions of highly soluble naphthalene diimide derivatives for neutral pH aqueous redox flow batteries, *Adv. Mater.* 35 (2023), <https://doi.org/10.1002/adma.202210859>.
- [38] P. Ledwon, D. Ovsianikova, T. Jarosz, S. Gogoc, P. Nitschke, W. Domagala, Insight into the properties and redox states of n-dopable conjugated polymers based on naphthalene diimide units, *Electrochim. Acta* 307 (2019) 525–535, <https://doi.org/10.1016/j.electacta.2019.03.169>.
- [39] J. Royakkers, K. Guo, D.T.W. Toolan, L. Feng, A. Minotto, D.G. Congrave, M. Danowska, W. Zeng, A.D. Bond, M. Al-Hashimi, T.J. Marks, A. Facchetti, F. Cacialli, H. Bronstein, Molecular encapsulation of naphthalene diimide (NDI) based π -conjugated polymers: a tool for understanding photoluminescence, *Angew. Chem. Int. Ed.* 60 (2021) 25005–25012, <https://doi.org/10.1002/anie.202110139>.
- [40] M.J. Frisch, G.W. Trucks, H.B. Schlegel, G.E. Scuseria, M.A. Robb, J.R. Cheeseman, G. Scalmani, V. Barone, G.a. Petersson, H. Nakatsuji, X. Li, M. Caricato, a. V. Marenich, J. Bloino, B.G. Janesko, R. Gomperts, B. Mennucci, H.P. Hratchian, J. V. Ortiz, a.F. Izmaylov, J.L. SonnenbergWilliams, F. Ding, F. Lipparini, F. Egidi, J. Goings, B. Peng, A. Petrone, T. Henderson, D. Ranasinghe, V.G. Zakrzewski, J. Gao, N. Rega, G. Zheng, W. Liang, M. Hada, M. Ehara, K. Toyota, R. Fukuda, J. Hasegawa, M. Ishida, T. Nakajima, Y. Honda, O. Kitao, H. Nakai, T. Vreven, K. Throssell, J.a. Montgomery Jr., J.E. Peralta, F. Ogliaro, M.J. Bearpark, J.J. Heyd, E.N. Brothers, K.N. Kudin, V.N. Staroverov, T.a. Keith, R. Kobayashi, J. Normand, K. Raghavachari, a.P. Rendell, J.C. Burant, S.S. Iyengar, J. Tomasi, M. Cossi, J. M. Millam, M. Klene, C. Adamo, R. Cammi, J.W. Ochterski, R.L. Martin, K. Morokuma, O. Farkas, J.B. Foresman, D.J. Fox, G16_C01, Gaussian 16, Revision C.01, Gaussian, Inc., Wallin, 2016.